Electrophoretic deposition of ZnO/alginate and ZnO-bioactive glass/alginate composite coatings for antimicrobial applications

Cordero-Arias, L; Cabanas-Polo, S; Goudouri, O.M; Misra, S.K; Gilabert, J; Valsami-Jones, Eugenia; Sanchez, E; Virtanen, S; Boccaccini, A.R

DOI:
10.1016/j.msec.2015.05.034

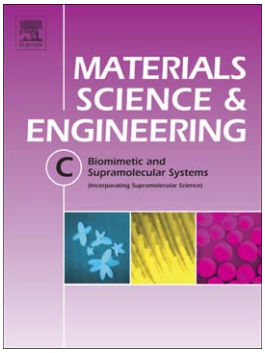

Electrophoretic deposition of ZnO/alginate and ZnO-bioactive glass/alginate composite coatings for antimicrobial applications

L. Cordero-Arias, S. Cabanas-Polo, O.M. Goudouri, S.K. Misra, J. Gilabert, E. Valsami-Jones, E. Sanchez, S. Virtanen, A.R. Boccaccini

PII: S0928-4931(15)30082-5
DOI: doi: 10.1016/j.msec.2015.05.034
Reference: MSC 5469

To appear in: *Materials Science & Engineering C*

Received date: 5 December 2014
Revised date: 20 February 2015
Accepted date: 8 May 2015

Please cite this article as: L. Cordero-Arias, S. Cabanas-Polo, O.M. Goudouri, S.K. Misra, J. Gilabert, E. Valsami-Jones, E. Sanchez, S. Virtanen, A.R. Boccaccini, Electrophoretic deposition of ZnO/alginate and ZnO-bioactive glass/alginate composite coatings for antimicrobial applications, *Materials Science & Engineering C* (2015), doi: 10.1016/j.msec.2015.05.034

Electrophoretic deposition of ZnO/alginate and ZnO-bioactive glass/alginate composite coatings for antimicrobial applications

L. Cordero-Arias[a], S. Cabanas-Polo[a], O. M. Goudouri[a], S.K. Misra[b], J. Gilabert[c], E. Valsami-Jones[d], E. Sanchez[c], S. Virtanen[e], A. R. Boccaccini[a]

[a]Institute of Biomaterials, Department of Materials Science and Engineering, University of Erlangen-Nuremberg, Cauerstrasse 6, D-91058 Erlangen, Germany

[b]Materials Science and Engineering, Indian Institute of Technology Gandhinagar, Ahmedabad 382424, India.

[c]Institute of Ceramics Materials (ITC), University Jaume I, Avenida Vicent SosBaynat 12006-Castellon, Spain

[d] School of Geography, Earth and Environmental Sciences, University of Birmingham, Edgbaston, Birmingham B15 2TT UK

[d]Institute for Surface Science and Corrosion (LKO, WW4), Department of Materials Science and Engineering, University of Erlangen-Nuremberg, Martensstrasse 7, D-91058 Erlangen, Germany

*Corresponding author email: aldo.boccaccini@ww.uni-erlangen.de

Abstract

Two organic/inorganic composite coatings based on alginate, as organic matrix, and zinc oxide nanoparticles (n-ZnO) with and without bioactive glass (BG), as inorganic components, intended for biomedical applications, were developed by electrophoretic deposition (EPD). Different n-ZnO (1–10 g/L) and BG (1-1.5 g/L) contents were studied for a fixed alginate concentration (2 g/L). The presence of n-ZnO was confirmed to impart antibacterial properties to the coatings against gram-negative bacteria *Escherichia coli*, while the BG induced the formation of hydroxyapatite on coating surfaces thereby imparting bioactivity, making the coating suitable for bone replacement applications. Coating composition was analyzed by thermogravimetric analysis (TG), Fourier transform infrared spectroscopy (FTIR), X-ray diffraction (XRD) and energy dispersive X-ray spectroscopy (EDS) analyses. Scanning electron microscopy (SEM) was employed to study both the surface and the cross section morphology of the coatings. Polarization curves of the coated substrates made in cell culture media at 37°C confirmed the corrosion protection function of the novel organic/inorganic composite coatings.

Keywords: ZnO nanoparticles, alginate, bioactive glass, coating, electrophoretic deposition (EPD)

1 Introduction

Around 1.5 million bone replacement surgical procedures per year are performed worldwide, with a cost of around US$10 billion [1]. Infection of orthopedic implants occurs in 5% of the cases for a total amount of 100.000 cases per year just in the USA [1]. This problem is originated by bacterial colonization of the implant surface where bacteria form a biofilm causing infection of the bone and surrounding tissues [2]. Bacteria can come from a variety sources: deficient hygienic standards in hospital [3], and also from the patient's own skin and/or mucosa, etc. [4,5]. These microorganisms attach to the implant surface in an irreversible way. After implantation bacteria can produce a relatively thick extracellular matrix layer on the implant surface leading to the formation of an adherent biofilm [4–6]. This biofilm makes difficult the penetration of antibacterial agents (e.g. immune cells or antibiotics) being thus extremely resistant and adhesive [5]. A chronic infection adjacent to the implant can lead to osteomyelitis, acute sepsis, and even death [7]. To tackle this problem, a solution being proposed is the incorporation of antibacterial coatings on the implant surface to prevent the biofilm formation.

Another common problem observed for metallic implants is its encapsulation by fibrous tissue [8], which leads to micromovements of the implant, migration and possible loosening [8,9]. To solve these problems a bioactive material can be used to coat the implant and in order to induce its osteointegration. Bioactive glasses are well-known biocompatible materials with osteoinductive properties that are being increasingly used in the orthopedic field to promote bone repair and regeneration [10–13]. Bioactive glasses form a hydroxyapatite surface layer where osteogenic cells can attach and differentiate [13–15] thereby improving the bone-implant contact and promoting bone in-growth. Moreover, bioactive silicate glasses of silicate show antibacterial, anti-inflammatory and angiogenic effects [16–18].

ZnO has been used in the production of solar cells, photovoltaic devices, batteries and biosensors mainly due its semiconducting properties [19–21]. This material has also been used to produce biomimetic membranes able to immobilize proteins due to its rapid transfer of electrons, which

represents an application of ZnO in the field of biomaterials [22]. Antibacterial properties of ZnO have been reported [23–25], which opens possible applications of this material in the production of a coating on metallic implants with antibacterial activity. Combining ZnO with a bioactive glass (e.g. 45S5 Bioglass®) [10], a new composite material can be developed that tackles simultaneously the two main challenges of traditional orthopedic implants: probability of infections and lack of osteointegration.

Spray plasma coating is a technology widely used to produce bioactive coatings on metallic implants, mainly based on calcium phosphates, e.g. hydroxyapatite [26]. However, due to the high temperatures reached during the process, a morphological change on the bioactive material is induced which may reduce its bioactivity. To solve this inconvenience, a new family of organic/inorganic composite coatings made by room temperature electrophoretic deposition (EPD) is emerging, where a biocompatible polymer and a bioactive glass (or ceramic) material are combined [27–32]. EPD has been used to produce pure bioactive glass coatings [33] and composite coatings of bioactive glass with different polymers [34,35] for orthopedic and dental applications. With this room temperature processing method possible degradation and microstructural damage of the coating and substrate, e.g. phase changes and microcracking due to thermal expansion mismatch, are avoided. A growing family of this type of organic-inorganic composite coatings is being produced, as reviewed elsewhere [27].

An interesting polymer for fabrication of organic/inorganic composite coatings with potential biomedical applications is alginate [36], which has been used only to a limited extent in combination with EPD to produce bioactive coatings [28,31,36,37]. Alginate is a natural polysaccharide which, due to its low toxicity and biocompatibility [38–40], has been studied for different applications, e.g. biosensors, drug delivery systems and tissue engineering. This polymer presents a potential binding effect with proteins, growth factors and bone-forming cells, being thus also attractive to develop coatings for bone contacting materials.

EPD appears as a versatile, simple and low cost technique to create highly homogeneous coatings with clear advantages, like the possibility to obtain homogeneous coatings on 3D structures of complex shape as well as on porous substrates [27,41,42]. Moreover, EPD enables production of a wide variety of coatings due to the possibility of depositing different types of materials and combination of materials, e.g. inorganic, polymeric and composite materials with high microstructural homogeneity and tailored thickness [27,41–43]. The EPD process is based on the application of an electric field between two conductive electrodes immersed in a colloidal suspension [43]. The electric field imparts electrophoretic motion to charged particles in suspension causing their movement to the oppositely charged electrode, where they deposit forming a coherent coating over it.

The aim of this research was to develop a new group of electrophoretic alginate-based coatings on stainless steel substrates incorporating ZnO nanoparticles and bioactive glass microparticles as inorganic phases. The deposition conditions (i.e. suspension concentration, electric field and deposition time) as well as the colloidal stability of the starting suspensions were investigated. Coating compositions were studied using XRD, FTIR and TG techniques. The electrochemical behavior was also evaluated by obtaining polarization curves of coated substrates to assess the protective effect of the coatings on the corrosion behavior of the stainless steel substrates. Antibacterial test against gram-negative bacteria were performed to evaluate the potential antibacterial properties of the coatings. Gram-negative bacteria were chosen for the tests because even if ZnO nanoparticles have been frequently tested against this type of bacteria, the effect of the presence of the alginate matrix and bioactive glass particles on antibacterial activity is unknown.

2 Materials and methods

2.1 Suspension preparation

Sodium alginate (Sigma Aldrich, Germany), zinc oxide nanoparticles (n-ZnO, Intrinsiq Materials, UK), bioactive glass (BG) microparticles (5-25 µm particle size) of 45S5 composition [10], deionized water

and ethanol were used to prepare the composite coatings. A 2 g/L alginate solution was used in all experiments while the ceramic content was varied from 1 to 10 g/L. At the same time, different n-ZnO/BG ratios were chosen, varying the n-ZnO content from 25 to 100 wt.%. Samples were labeled ZA (100 wt.% ZnO), 50-ZBA (50 wt.% ZnO and 50 wt.% BG) and 25-ZBA (25 wt.% ZnO and 75 wt.% BG). In order to avoid hydrogen evolution formation during the EPD process (due to water electrolysis) a mixture of 40 vol.% ethanol – 60 vol.% water was used [31,37]. To achieve an adequate dispersion of the components, the suspensions were magnetically stirred for 10 min followed by 60 min of ultrasonication (using an ultrasonic bath, Bandelin Sonorex, Germany). Zeta-potential measurements were carried out in order to analyze the colloidal stability of the suspensions. These measurements were done by Laser Doppler Velocimetry (LDV) technique using a Zetasizer nano ZS equipment (Malvern Instruments, UK). The solid content of all suspensions was adjusted to 0.1 g/L in order to ensure reliable measurements.

2.2 Electrophoretic deposition

Stainless steel AISI 316L electrodes (foils of 2.25 cm^2 deposition area and 0.2mm thickness) were used to deposit the coatings via constant voltage-EPD. The distance between the electrodes in the EPD cell was kept constant at 10 mm. Deposition voltages and times in the ranges 5-40 V and 5-35 s, respectively, were studied. The deposition yield was evaluated using an analytical balance (precision 0.0001g). Coated substrates were dried during 24 h in normal air at room temperature prior to mass determination.

2.3 Characterization

In order to characterize the coatings, XRD (D8 Philips X'PERT PW 3040 MPD), FTIR (Bruker Instruments, Germany) and thermogravimetric (TG) (TGA/SDTA 851e, Mettler Toledo) tests in air (heating rate: 10°C/min) were performed. The microstructure of the ZnO nanoparticles was characterized with TEM (JEOL 2100, 200 kV). The surface microstructure and composition of the coatings were analyzed by SEM (Hitachi S4800) and energy-dispersive X-ray spectroscopy (EDX), respectively. To determine the coating thickness, cross section of the samples were cut using and ion

mill (Hitachi IM4000) and further observed by SEM. Bending tests were also performed in order to qualitatively evaluate the deformation ability of the coatings and the adhesion between the substrate and the coating.

2.4 Electrochemical behavior and corrosion

The electrochemical behavior of the coatings was studied in order to test their possible corrosion protective properties. Potentiodynamic polarization curves were obtained using a potentiostat/galvanostat (Autolab PGSTAT 30). The samples were immersed in 100 mL of Dulbecco´s MEM (DMEM, Biochrom) at 37°C. A conventional three electrode system was used, where a platinum foil served as counter electrode and Ag/AgCl (3M KCl) was used as reference electrode. The analysis was carried out using an O-ring cell with an exposed sample area of 0.38 cm^2 with a potential sweep rate of 1 mV/s.

2.5 Bioactivity in-vitro assessment

The bioactivity of the coatings was determined through immersion in simulated body fluid (SBF) using Kokubo's protocol [44]. The samples with an area of 2.25 cm^2 were immersed in 50 mL SBF (pH = 7.4) during 7 days at 37°C. XRD was used to evaluate the formation of hydroxyapatite (HA) on the coatings.

2.6 Antibacterial evaluation

The antibacterial activity of all samples was investigated against the gram-negative *Escherichia coli* (*E. coli, strain:* dH5a) using the following method. A colony of *E. coli* was cultivated at 37 °C for 24 h in 5 mL of Lactose broth (LB) medium supplemented with 0.1 vol.% of Ampicillin. After 24 h, the cultures were diluted in 10 ml of LB medium. 60 µL of the bacterial solution was added on each coated sample and incubated for 1, 2, 3 and 4 h at 37 °C. After the specific time points, each sample was stamped on the surface of a LB-agar solid culture, which was prepared by dissolving 7 g of agar and 9 g of LB in 500 mL of water, poured onto a plastic petri dish for gelation, and cultivated at 37 °C for 24 h.

3 Results and Discussion

3.1 Solution stability, electrophoretic deposition and characterization

The compatible interaction of water with the body in comparison with other solvents, makes it a simple and reasonable choice to be used as dispersing medium for EPD suspensions. However water leads to hydrogen and oxygen evolution at relatively low voltages inducing a negative effect in the adhesion and homogeneity of the electrophoretic coatings [43]. To avoid possible negative effects, a mixture of 60 vol.% water and 40 vol.% ethanol was used based on our previous work [31,37] with an alginate content of 2 g/L. The ethanol contributes to reduce and in best case to suppress hydrogen formation during deposition.

Table 1 presents the results of the zeta potential values for different suspensions (a solid content of 0.1 g/L was used to ensure reliable measurements with a ceramic/polymer ratio of 1). As it can be seen ZnO nanoparticles have a positive zeta potential which predicts a cathodic deposition, however the high standard deviation reflects certain instability of the system. The addition of alginate to the suspension shifts the zeta potential to negative values, as expected, considering that the alginate is an anionic biopolymer which develops a negative charge in solution. The shift of the zeta potential to negative values implies the anodic deposition of the sample ZA. When BG is also introduced in the suspension (samples 50-ZBA and 25-ZBA), the zeta potential remains negative and becomes slightly higher (in absolute value), which implies a higher suspension stability. Moreover, the change in the ratio BG/n-ZnO did not induce changes in the zeta potential. Considering the low zeta potential values of the BG and the BG/n-ZnO suspensions in the absence of alginate, it could be considered that the stability of the particles in suspension is mainly controlled by the alginate. This could be explained by the fact that the negatively charged alginate is being absorbed on the particles surface, and therefore it is responsible for the high zeta-potential values measured.

Table 1 Zeta potential values of different suspensions

Suspension	Zeta-potential (mV)
n-ZnO (without Alg)	24±19
BG (without Alg)	-17±13
BG-n-ZnO (75wt%/25wt%)	-19±12
ZA	-58±9
50-ZBA	-65±10
25-ZBA	-65±9

To optimize the system, an initial n-ZnO content of 2 g/L was chosen keeping a ceramic (BG and ZnO)/polymer weight ratio of 1:1. Homogeneous and crack-free coatings were obtained using 30 V of deposition potential and 5 s of deposition time. Higher voltages or times led to cracking of the coating mainly due to the hydrogen evolution during the deposition, while lower voltages or times led to inhomogeneous coatings. For ceramic contents from 1 to 10 g/L, which implies ceramic/polymer weight ratios ranging from 0.5 to 5, determined deposition conditions (30 V and 5 s) were found to be optimum, leading also to homogeneous and crack-free coatings. This is an important finding considering that in other works with metallic oxide nanoparticles, when the ceramic/polymer ratio was above 3, the coatings were full of cracks and presented poor adhesion to the substrate [37,45]. Fig. 1 shows the surface of ZA and 25-ZBA coatings produced with different ceramic contents (2 and 10 g/L). Images documenting the results of the bending are also presented in Fig. 1. As it can be observed, even for 10 g/L the coatings resisted the bending process with just some small cracks located at the borders of the sample. These cracks at the edges of the substrates are due to the higher ceramic content deposited in such areas as a consequence of the well-known edge effect during EPD [45].

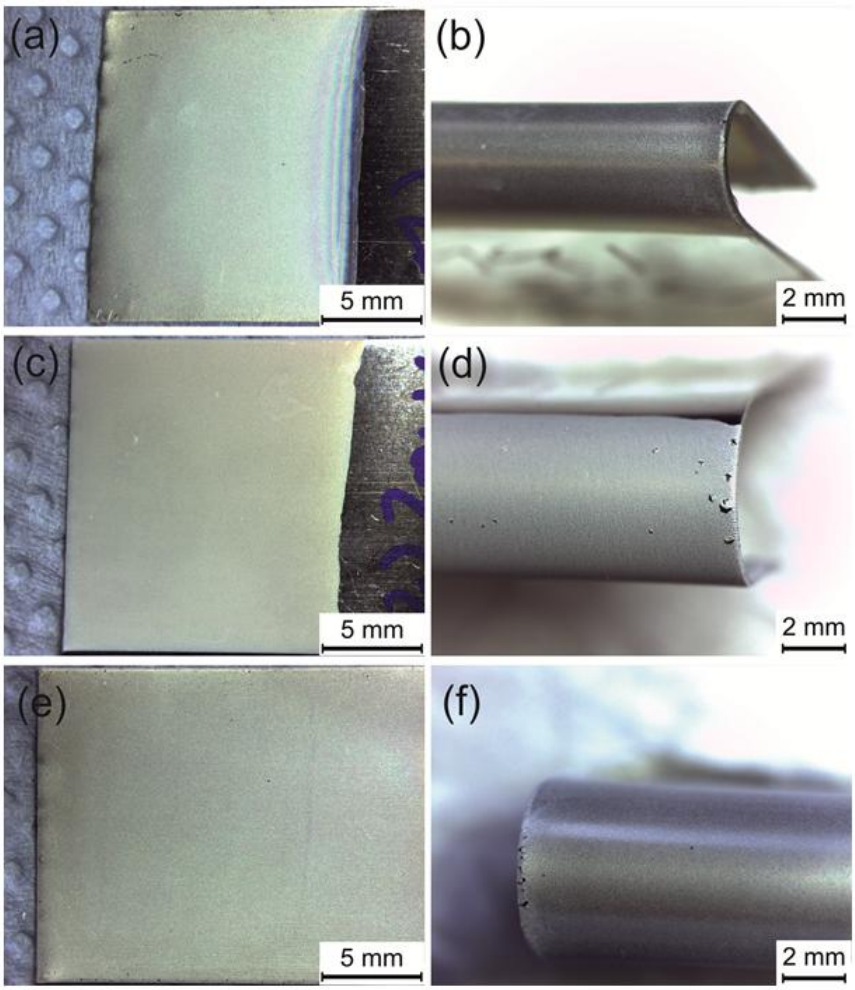

Figure 1 Coatings obtained at 30 V and 5 s of deposition time from the system ZA with 2g/L (a and b) and 10 g/L (c and d) of ceramic content, and from the system 25-ZBA with 2 g/L of ceramic content (e and f).

Fig. 2 (*a* and *b*) presents the TEM and SEM images of the ZnO nanoparticles. As it can be observed, the particles have a broad size distribution with sizes ranging from tens to hundreds of nanometers, and presented an elongated hexagonal shape, typical of ZnO powders which crystallize in a hexagonal crystalline phase, called zincite, as further confirmed by XRD. Fig. 2 (*c* and d) shows the SEM images of the ZA coatings produced with different ceramic contents (4 and 10 g/L). As it can be observed, in all cases the coatings are fully homogeneous in the microscale and no cracks are observed with deposited particles of size between 20 and 60 nm, meaning that the large ZnO particles (seen by TEM) in suspension do not participate in the coating formation. As a consequence of their larger particle size, their electrophoretic mobility is lower and these particles probably settle

down due to gravity forces. The coating thickness was around 3-4 µm for a ZA coating produced with 2g/l ZnO.

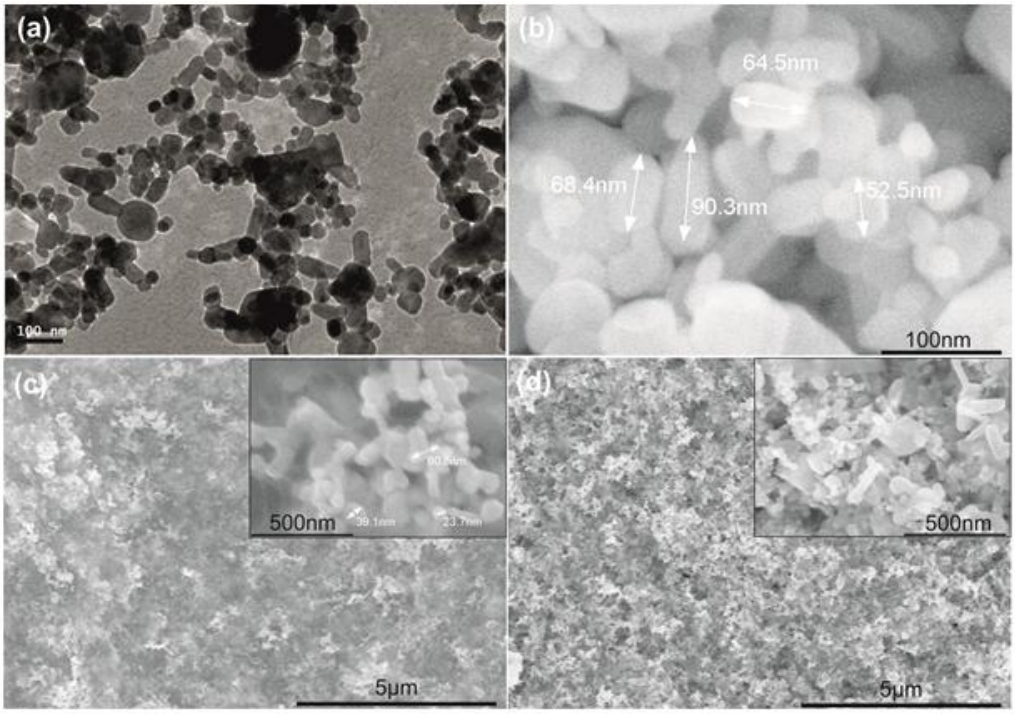

Figure 2 TEM and SEM images of the ZnO nanoparticles (a and b) and SEM images of the ZA coating produced from a suspension of 4 g/L (c) and 10 g/L (d) of ceramic (BG, ZnO) content.

Fig. 3 shows the variation of deposition yield of ZA coating as a function of the n-ZnO particles concentration in suspension. As it can be observed, the higher the concentration, the higher is the deposition yield. Also at higher concentrations (more than 8 g/L) the system presents an asymptotic behavior indicating the system´s incapacity to have higher deposition yields, and supporting the fact that the deposition is controlled by the presence of alginate. When the ceramic content is increased but the alginate content is kept constant (2 g/L), the ratio polymer/ceramic decreases considerably, from 2 when using 1 g/L of n-ZnO to 0.2 when the n-ZnO content is 10 g/L. Although the saturation point of n-ZnO powders with alginate has not been measured in this study, it is likely that at such a low polymer/ceramic weight ratio as 0.2, the ZnO particles would present a lower zeta potential value and therefore agglomerates could form more easily. At the same time, with high ceramic

contents, particle-particle interactions become more important and the largest ZnO particles, as well as the agglomerates, tend to settle down not reaching the deposition electrode.

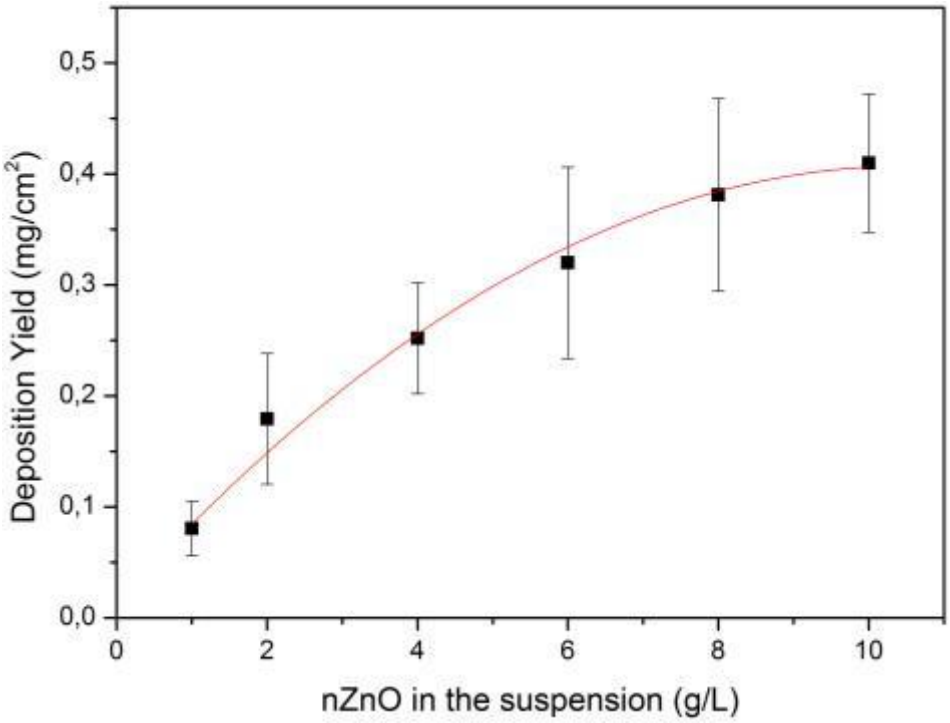

Figure 3 Relationship between n-ZnO concentration in suspension and deposited mass per area using 2 g/L alginate suspensions in ethanol/water solvent. Deposition time was 5 s and deposition potential 30 V.

Different coatings containing BG and n-ZnO were obtained varying the deposition voltage and time (from 5 to 60 V and from 1 s to 5 min respectively) and it was observed that the optimal conditions were the same used for the ZA system, i.e. 5 s deposition time and a voltage of 30 V. The fact that both systems exhibit the same optimal conditions may be due to the fact that the deposition is controlled by the alginate. According to the zeta potential measurements, we suggest that the alginate is adsorbed on the surface of both BG and n-ZnO particles, which increases the absolute value of the zeta potential. However, the non-absorbed chains of the alginate in the suspension are also affected by the applied electric field since alginate is a polyelectrolyte which is negatively charged in the media. Under these conditions, when the voltage is applied, the particles with adsorbed alginate will move along with the free polymer chains. It is suggested that these free chains can further favor the deposition on the electrode by dragging the ceramic particles towards the

deposition electrode. As the alginate concentration is constant for each experiment, it can be considered that the kinetics of deposition is determined by the mobility of the polymer molecules. In the proposed mechanism, alginate forms a charged polymer cloud in the suspension and with its movement, due to the applied potential, it involves the ceramic particles forming the composite coating on the electrode surface. Fig. 4a presents the SEM image of 25-ZBA coating produced with a ceramic content of 2 g/L. As it can be seen, the coatings are homogeneous with BG particles well distributed on the surface. Fig 4 (b and c) shows a BG particle partially covered with ZnO particles, which confirms the co-deposition of both materials. Fig. 4d shows the EDX results of large particles deposited, where the presence of Si, P, Ca and Na can be confirmed, indicating that these are BG particles. Carbon is coming from the polymer as well from the stainless steel substrate. While Ni, S, Cr and Fe are also from the substrate and Zn confirms the presence of the ZnO nonoparticles. Homogeneous and crack-free coatings were obtained. ZBA coatings also showed sufficient adhesion to the substrate after the qualitative bending test carried out (Fig. 2 (e and f)). ZBA coatings exhibed an average thickness of 2-3 µm.

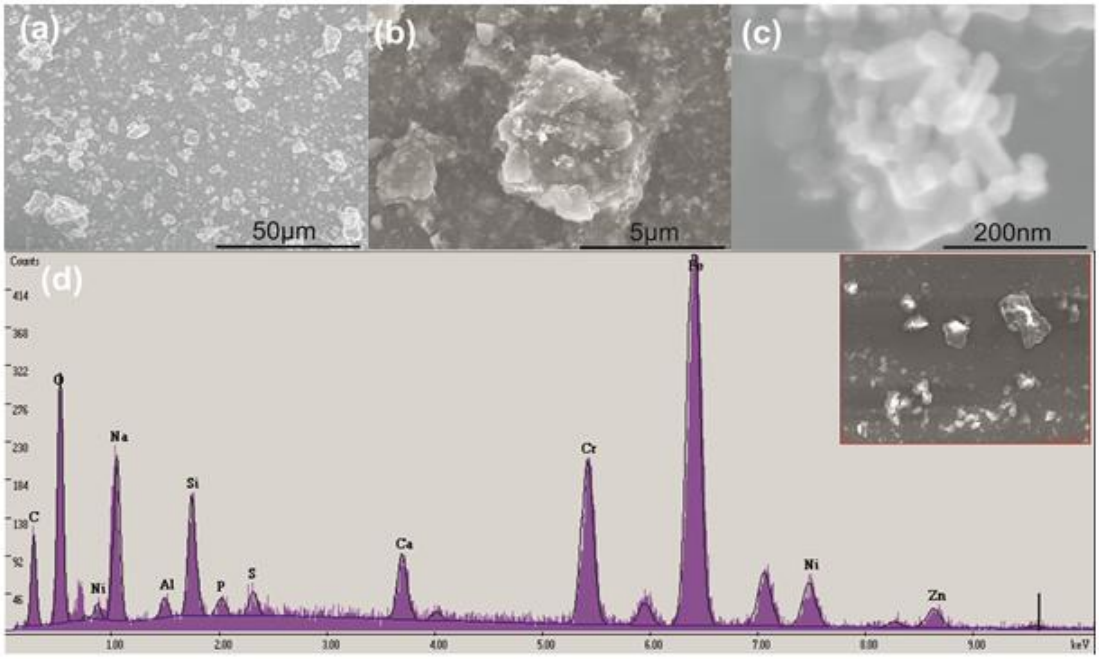

Figure 4 SEM images (a, b and c) and EDX results (d) of the n-ZnO-BG/Alg coating produced from a suspension of 2g/l ceramic components (25wt.% n-ZnO and 75wt.%BG).

Fig. 5 shows the FTIR results for both ZA and 25-ZBA coatings produced from a suspension with 2g/L of ceramic content, pure alginate coating and inorganic powder, i.e. BG powder and n-ZnO powder. The presence of alginate in ZA and ZBA coatings is confirmed by the characteristic peaks of both the asymmetric and the symmetric stretching of COO^- group at 1620 cm^{-1} and 1413 cm^{-1}, respectively [46]. In the case of pure alginate coating, an extra peak at 1723 cm^{-1}, caused by the stretching vibration of the protonated carboxylic group of alginic acid, is observed [36,47]. When BG and n-ZnO particles are included in the suspension, an alkalinisation effect occurs and the pH increases resulting in the deprotonation of the mentioned carboxylic group. Therefore, the peak at 1723 cm^{-1} does not appear in the ZA and 25-ZBA coatings. The BG powder spectrum shows the characteristic asymmetric stretching and bending peaks of the Si-O-Si bonds at ~1043, 924 and 497-500 cm^{-1} [48], respectively. The presence of ZnO was confirmed by EDX and XRD.

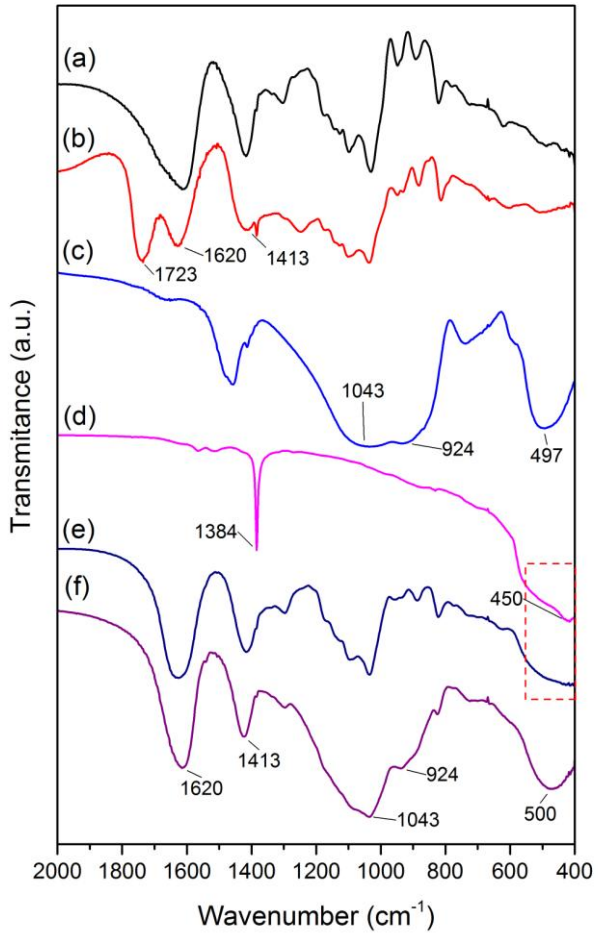

Figure 5 FTIR results for the different coatings and their components. Alginate powder (a), alginate coating (b), BG powder (c), ZnO powder (d), ZA coating (e) and 25-ZBA coating (f).

The thermal behavior of the ZA and 25-ZBA composite coatings was analyzed by TG/DTA measurements (Fig. 6). The first mass loss in the TG curve at around 100°C can be attributed to the physically adsorbed water that was retained in the coatings. Between 300 and 450°C, an exothermic peak in the DTA curves is observed for all the coatings (not shown), which can be attributed to the burn out of the alginate [28,31]. Once the alginate is burned out, there is no other important change in the mass loss (at T>500°C), indicating that the residual material in the coating is the (non-burnable) ceramic phase. Table 1 shows the final composition of the coatings, which is based on the thermal analysis results.

Table 1 Final composition of the coatings from both systems (ZA and 25-ZBA) according to the TG analysis.

System	Initial ceramic content in suspension (g/L)	Final components in the coating					
		Water		Alginate		Ceramic phase	
		wt.%	vol.%	wt.%	vol.%	wt.%	vol.%
ZA	2	12	4	35	15	53	81
	10	4	1	13	4	83	95
25-ZBA	2	13	7	27	24	60	69

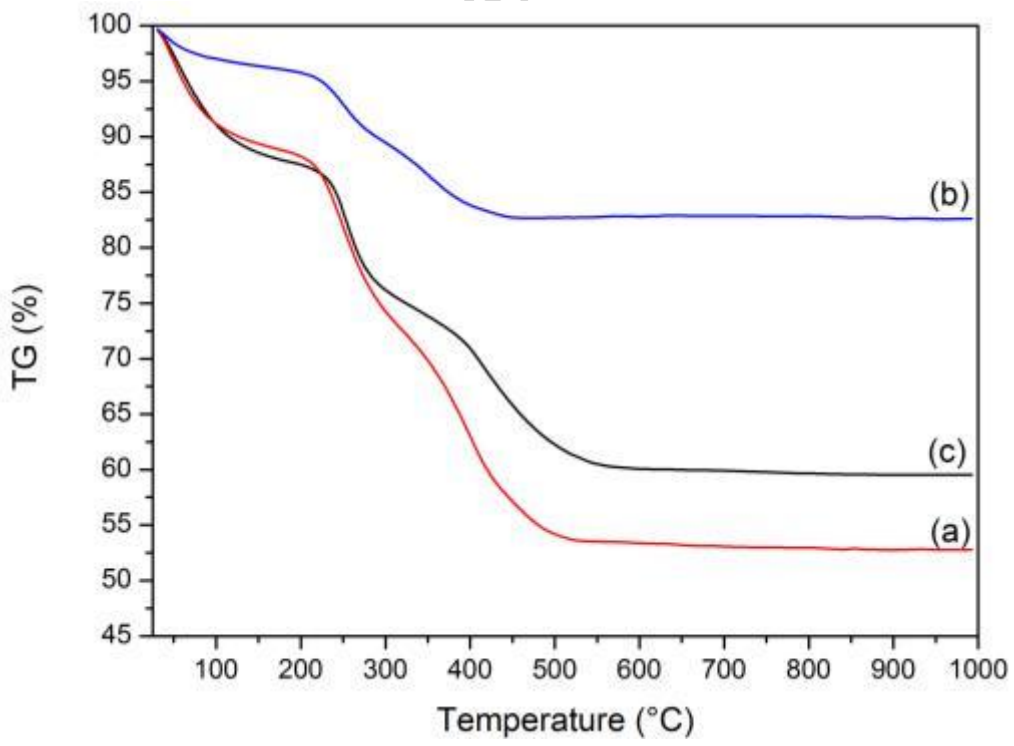

Figure 6 Thermogravimetric analysis for the ZA coating produced from suspensions with 2g/L (a) and 10g/L (b) of ceramic content and for the 25-ZBA coating produced from a suspension coatining 2g/L of ceramic (c).

3.1 Electrochemical behavior and corrosion

The corrosion resistance of metallic materials used in biological environments is one of the key parameters determining their success. Applying a protective coating is one of the alternatives to

tackle the relatively low corrosion resistance of stainless steel in biological fluids, which is due to the high chloride content in this environment. Fig. 7 shows the polarization curves of the uncoated 316L stainless steel substrate (bare metal), the ZA composite with two different solid contents, namely 1 g/L and 10 g/l, and also 50-ZBA and 25-ZBA coatings produced with 2 g/L of ceramic content in the suspension. It can be observed that all coated samples show a higher E_{corr} and a lower i_{corr} compared to the bare metal, indicating that both composite coatings protect the substrate against corrosion. The ZA coatings exhibit a higher E_{corr} and lower i_{corr} than the 50-ZBA and 25-ZBA coatings, which is likely due to the presence of the BG particles that increase the activity of the system due to the dissolution of the material in the DMEM. The BG dissolution leaves space to the liquid media to penetrate into the coating increasing the current density. Similar phenomena were previously reported on related BG containing composite coatings [37].

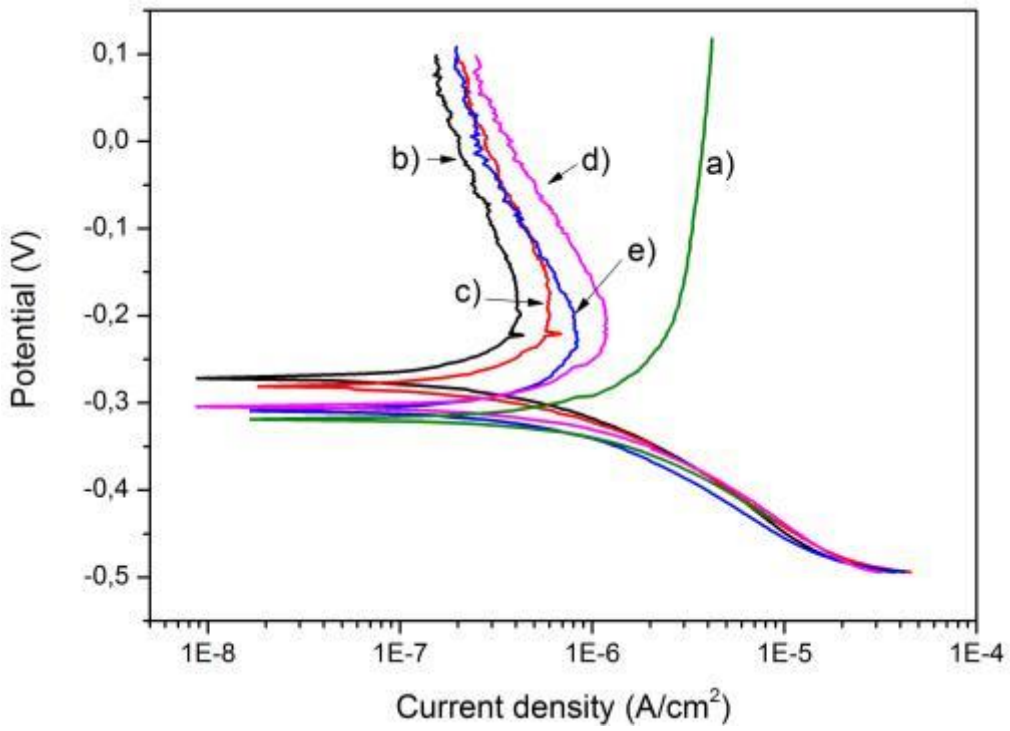

Figure 7 Polarization curves obtained using DMEM at 37°C for: the bare SS 316L (a), ZA coatings produced from suspension with 1 g/L (b) and 10 g/L (c) of ceramic content, also 50-ZBA (d) and 25-ZBA (e) coatings produced from a suspensions with 2 g/L of ceramic particles

3.2 Bioactivity in-vitro assessment

In order to evaluate the potential bioactivity of ZA and ZBA coatings, samples prepared from suspensions with solid concentration of 2 g/L were immersed in SBF at 37°C during 7 days. Fig. 8 (diffractograms b and c) shows the normalized XRD plots of ZA and ZBA coatings obtained after immersion in SBF. As expected the ZA coating was not bioactive, e.g. no hydroxyapatite (HA) was formed on the coating surfaces. On the other hand the coating with BG was able to form a HA layer over it, indicating that the presence of the n-ZnO particles did not inhibit the bioactivity of the BG. As it can be seen, the ZBA coating presents the typical diffraction peaks corresponding to the (100), (200), (111) (211), (221) and (222) planes of hydroxyapatite (HA), indexed using the JCPDS (card number 09-0432) the characteristic peak at 31,8° corresponding to HA is overlapped with a peak of ZnO, but this peak is clearly more intense than in the other two diffractograms, indicating the presence of ZnO and HA.

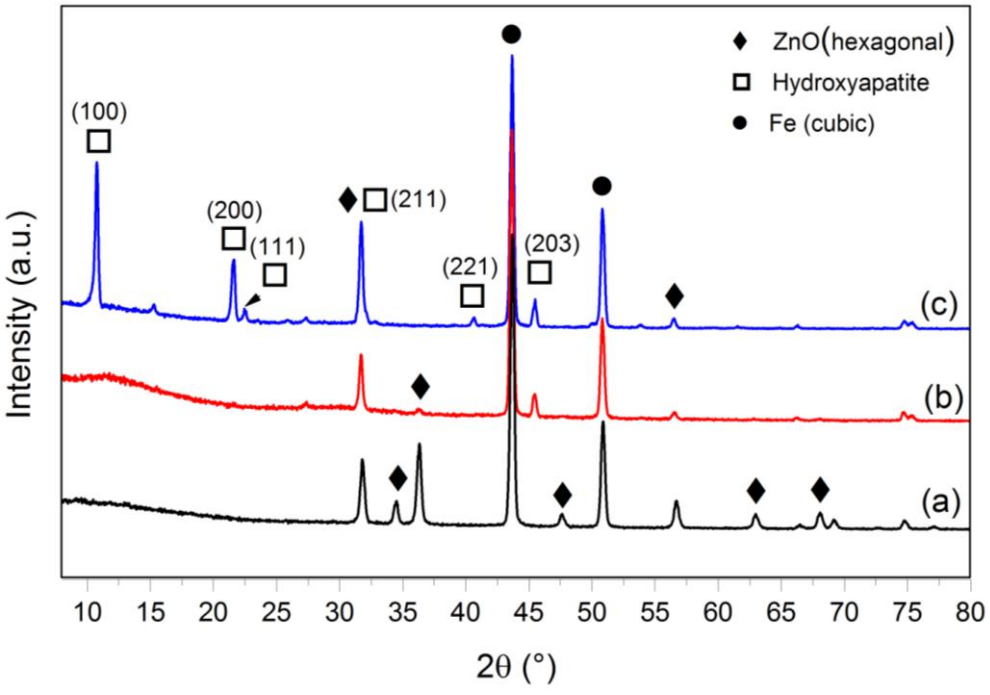

Figure 8 Normalized XRD results of the samples: ZA coating produced using a suspension with 2g/L of ceramic content (a), ZA coating produced for a suspension with 2g/L of ceramic content and after 7 days of immersion in SBF (b) and 25-ZBA coating produced for a suspension with 2 g/L of ceramic content and after 7 days of immersion in SBF (c). JCPDS cards: 09-0432 (HA), 033-0945 (austenitic stainless steel) and 036-1451 (ZnO).

3.3 Antibacterial evaluation

The antibacterial properties of the coatings were evaluated against the gram-negative *Escherichia coli* bacteria. To run the test four different samples were prepared: ZA and 25-ZBA coatings, stainless steel substrate as a reference and a coating containing only BG and alginate (BG/Alg sample) [31], also as reference, to evaluate the effect of the BG. The antibacterial activity of the coated samples against E. coli is illustrated in Fig. 9. Each picture displays four different areas corresponding to the four different time points considered (1, 2, 3 and 4 h). As observed in fig. 9 (a and b), there is no evident reduction of the bacterial colonies on the stainless steel substrate or on the BG/Alg sample even after 4 h. On the other hand, for sample ZA (fig. 9c) the bacterial colonies have clearly disappeared after just 1 h, which is an indication of the antibacterial power of the n-ZnO particles. Finally, in the case of the coatings obtained with both BG and n-ZnO powders (sample 25-ZBA), the bacterial colonies do not disappear completely but they are significantly reduced after 3 h and especially after 4 h (fig. 9d). The key difference between samples ZA and 25-ZBA is the higher amount of ZnO nanoparticles present in sample ZA compared to sample 25-ZBA, which indicates that with increasing n-ZnO content, the antibacterial capability against gram-negative *Escherichia coli* bacteria increases. Antibacterial activity of ZnO against gram-positive and gram-negative bacteria has been already reported [49–51], especially against *Escherichia coli* [24]. The benefits of using small (nanoscale) particle size to increase antibacterial activity have been also reported [52,49]. The mechanism of antibacterial activity of ZnO is not yet fully understood [24]. Some authors ascribe the antibacterial activity to the generation of hydrogen peroxide [51,53,54], this idea has been partially confirmed [24]. On the other hand it has been also proposed that a binding of the ZnO particles to the cells due to electrostatic forces can damage the cell membrane killing the bacteria [55].

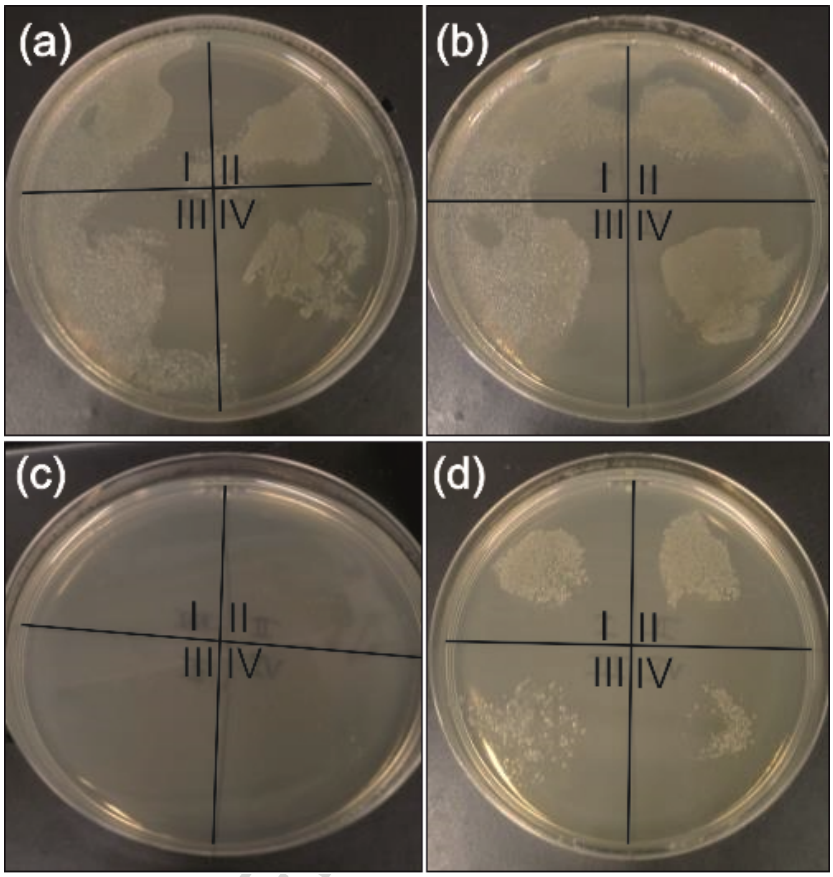

Figure 9 Antibacterial results of different coating against gram-negative E- Coli. Stainless steel (a), BG/Alg coating (1.5g/L BG) (b), ZA coating (c) and 25-ZBA coating (d). Zones I, II, II and IV indicate the number of hours that the test was run (1, 2, 3 and 4h respectively).

4 Conclusions

Novel ZnO/alginate and ZnO-BG/alginate composite coatings on stainless steel have been successfully obtained by anodic electrophoretic deposition. For both coatings optimized deposition conditions were 5 s and 30 V, as deposition time and potential, respectively. Homogeneous and crack free ZnO/alginate coatings can be obtained using suspensions with solid contents varying from 1 to 10 g/L. In terms of corrosion protection all coated samples presented a lower corrosion current density, with a slightly higher corrosion potential compared with the bare material, indicating the protective character of the coatingsagainst corrosion. The presence of BG in the coating induced the growth of a hydroxyapatite layer on the coating after 7 days of immersion in SBF. It was also proven that the presence of n-ZnO does not affect the development of the bone-like HA phase. Furthermore,

the incorporation of ZnO nanoparticles within the composite coatings clearly provides antibacterial properties against gram-negative *Escherichia coli* to the final material. Considering the corrosion protection properties as well as the bioactivity and antibacterial effect of the ZnO containing coatings, it can be concluded that these coatings provide a new alternative to tackle the main problems of bone replacement implants namely lack of osteointegration and infection risk.

Acknowledgments

L. Cordero-Arias thanks the German Academic Exchange Service (DAAD) for a scholarship. Dr. S. Cabanas-Polo acknowledges the financial support from the EU ITN FP-7 project GlaCERCo. The authors acknowledge Anja Friedrich, Ulrike Marten-Jahns, Helga Hildebrand and Elias Palpanes for experimental support and Intrinsiq Materials Ltd. (UK) for supplying the ZnO nanoparticles.

Appendices

References

[1] B.M. Holzapfel, J.C. Reichert, J.-T. Schantz, U. Gbureck, L. Rackwitz, U. Nöth, et al., How smart do biomaterials need to be? A translational science and clinical point of view, Adv. Drug Deliv. Rev. 65 (2012) 581–603. doi:10.1016/j.addr.2012.07.009.

[2] A. Gristina, P. Naylor, Q. Myrvik, Biomaterial-Centered Infections: Microbial Adhesion versus Tissue Integration, in: T. Wadström, I. Eliasson, I. Holder, Å. Ljungh (Eds.), Pathog. Wound Biomater. Infect. SE - 25, Springer London, 1990: pp. 193–216. doi:10.1007/978-1-4471-3454-1_25.

[3] D. Campoccia, L. Montanaro, C.R. Arciola, The significance of infection related to orthopedic devices and issues of antibiotic resistance, Biomaterials. 27 (2006) 2331–9. doi:10.1016/j.biomaterials.2005.11.044.

[4] R.M. Donlan, J.W. Costerton, Biofilms: survival mechanisms of clinically relevant microorganisms, Clin. Microbiol. Rev. 15 (2002) 167–193.

[5] G. Colon, B.C. Ward, T.J. Webster, Increased osteoblast and decreased Staphylococcus epidermidis functions on nanophase ZnO and TiO2, J. Biomed. Mater. Res. Part A. 78A (2006) 595–604. doi:10.1002/jbm.a.30789.

[6] P.K. Singh, M.R. Parsek, E.P. Greenberg, M.J. Welsh, A component of innate immunity prevents bacterial biofilm development, Nature. 417 (2002) 552–555.

[7] S.E. Cramton, C. Gerke, F. Gotz, In vitro methods to study staphylococcal biofilm formation., Methods Enzymol. 336 (2001) 239–255.

[8] S.B. Goodman, Z. Yao, M. Keeney, F. Yang, The future of biologic coatings for orthopaedic implants, Biomaterials. 34 (2013) 1–10. doi:10.1016/j.biomaterials.2013.01.074.

[9] H.T. Aro, J.J. Alm, N. Moritz, T.J. Mäkinen, P. Lankinen, Low BMD affects initial stability and delays stem osseointegration in cementless total hip arthroplasty in women: A 2-year RSA study of 39 patients, Acta Orthop. 83 (2012) 107–114. doi:10.3109/17453674.2012.678798.

[10] L.L. Hench, Biomaterials: a forecast for the future, Biomaterials. 19 (1998) 1419–1423. doi:http://dx.doi.org/10.1016/S0142-9612(98)00133-1.

[11] P. Ducheyne, Q. Qiu, Bioactive ceramics: the effect of surface reactivity on bone formation and bone cell function., Biomaterials. 20 (1999) 2287–2303.

[12] S. Lopez-Esteban, E. Saiz, S. Fujino, T. Oku, K. Suganuma, A.P. Tomsia, Bioactive glass coatings for orthopedic metallic implants, J. Eur. Ceram. Soc. 23 (2003) 2921–2930. doi:http://dx.doi.org/10.1016/S0955-2219(03)00303-0.

[13] I.D. Xynos, A.J. Edgar, L.D.K. Buttery, L.L. Hench, J.M. Polak, Ionic Products of Bioactive Glass Dissolution Increase Proliferation of Human Osteoblasts and Induce Insulin-like Growth Factor II mRNA Expression and Protein Synthesis, Biochem. Biophys. Res. Commun. 276 (2000) 461–465. doi:http://dx.doi.org/10.1006/bbrc.2000.3503.

[14] M.S. Bahniuk, H. Pirayesh, H.D. Singh, J. a Nychka, L.D. Unsworth, Bioactive glass 45S5 powders: effect of synthesis route and resultant surface chemistry and crystallinity on protein adsorption from human plasma., Biointerphases. 7 (2012) 41. doi:10.1007/s13758-012-0041-y.

[15] W. Cao, L.L. Hench, Bioactive materials, Ceram. Int. 22 (1996) 493–507. doi:10.1016/0272-8842(95)00126-3.

[16] N. Drnovšek, S. Novak, U. Dragin, M. Čeh, M. Gorenšek, M. Gradišar, Bioactive glass enhances bone ingrowth into the porous titanium coating on orthopaedic implants., Int. Orthop. 36 (2012) 1739–45. doi:10.1007/s00264-012-1520-y.

[17] D. Zhang, O. Leppäranta, E. Munukka, H. Ylänen, M.K. Viljanen, E. Eerola, et al., Antibacterial effects and dissolution behavior of six bioactive glasses, J. Biomed. Mater. Res. Part A. 93A (2010) 475–483. doi:10.1002/jbm.a.32564.

[18] A.A. Gorustovich, J.A. Roether, A.R. Boccaccini, Effect of bioactive glasses on angiogenesis: a review of in vitro and in vivo evidences, Tissue Eng. Part B. Rev. 16 (2010) 199–207. doi:10.1089/ten.TEB.2009.0416.

[19] Y. Li, K. Wu, I. Zhitomirsky, Electrodeposition of composite zinc oxide–chitosan films, Colloids Surfaces A Physicochem. Eng. Asp. 356 (2010) 63–70. doi:http://dx.doi.org/10.1016/j.colsurfa.2009.12.037.

[20] B.X. Gu, C.X. Xu, G.P. Zhu, S.Q. Liu, L.Y. Chen, X.S. Li, Tyrosinase immobilization on ZnO nanorods for phenol detection, J. Phys. Chem. B. 113 (2009) 377–381. doi:10.1021/jp808001c.

[21] Z.L. Wang, Zinc oxide nanostructures: growth, properties and applications, J. Phys. Condens. Matter. 16 (2004) R829–R858. doi:10.1088/0953-8984/16/25/R01.

[22] L. V. Trandafilović, D.K. Božanić, S. Dimitrijević-Branković, A.S. Luyt, V. Djoković, Fabrication and antibacterial properties of ZnO-alginate nanocomposites, Carbohydr. Polym. 88 (2012) 263–269. doi:10.1016/j.carbpol.2011.12.005.

[23] G. Appierot, A. Lipovsky, R. Dror, N. Perkas, Y. Nitzan, R. Lubart, et al., Enhanced antibacterial actiwity of nanocrystalline ZnO due to increased ROS-mediated cell injury, Adv. Funct. Mater. 19 (2009) 842–852. doi:10.1002/adfm.200801081.

[24] L. Zhang, Y. Jiang, Y. Ding, M. Povey, D. York, Investigation into the antibacterial behaviour of suspensions of ZnO nanoparticles (ZnO nanofluids), J. Nanoparticle Res. 9 (2007) 479–489. doi:10.1007/s11051-006-9150-1.

[25] J. Sawai, Quantitative evaluation of antibacterial activities of metallic oxide powders (ZnO, MgO and CaO) by conductimetric assay., J. Microbiol. Methods. 54 (2003) 177–182. doi:10.1016/S0167-7012(03)00037-X.

[26] M.E. Furth, A. Atala, M.E. Van Dyke, Smart biomaterials design for tissue engineering and regenerative medicine, Biomaterials. 28 (2007) 5068–5073. doi:http://dx.doi.org/10.1016/j.biomaterials.2007.07.042.

[27] A.R. Boccaccini, S. Keim, R. Ma, Y. Li, I. Zhitomirsky, Electrophoretic deposition of biomaterials, J. R. Soc. Interface. 7 Suppl 5 (2010) S581–613. doi:10.1098/rsif.2010.0156.focus.

[28] D. Zhitomirsky, J.A. Roether, A.R. Boccaccini, I. Zhitomirsky, Electrophoretic deposition of bioactive glass/polymer composite coatings with and without HA nanoparticle inclusions for biomedical applications, J. Mater. Process. Technol. 209 (2009) 1853–1860. doi:10.1016/j.jmatprotec.2008.04.034.

[29] K. Grandfield, I. Zhitomirsky, Electrophoretic deposition of composite hydroxyapatite–silica–chitosan coatings, Mater. Charact. 59 (2008) 61–67. doi:10.1016/j.matchar.2006.10.016.

[30] F. Sun, X. Pang, I. Zhitomirsky, Electrophoretic deposition of composite hydroxyapatite–chitosan–heparin coatings, J. Mater. Process. Technol. 209 (2009) 1597–1606. doi:10.1016/j.jmatprotec.2008.04.007.

[31] Q. Chen, L. Cordero-Arias, J.A. Roether, S. Cabanas-Polo, S. Virtanen, A.R. Boccaccini, Alginate/Bioglass® composite coatings on stainless steel deposited by direct current and alternating current electrophoretic deposition, Surf. Coatings Technol. 233 (2013) 49–56. doi:http://dx.doi.org/10.1016/j.surfcoat.2013.01.042.

[32] Z. Zhang, T. Jiang, K. Ma, X. Cai, Y. Zhou, Y. Wang, Low temperature electrophoretic deposition of porous chitosan/silk fibroin composite coating for titanium biofunctionalization, J. Mater. Chem. 21 (2011) 7705–7713.

[33] D. Krause, B. Thomas, C. Leinenbach, D. Eifler, E.J. Minay, A.R. Boccaccini, The electrophoretic deposition of Bioglass® particles on stainless steel and Nitinol substrates, Surf. Coatings Technol. 200 (2006) 4835–4845. doi:10.1016/j.surfcoat.2005.04.029.

[34] A.R. Boccaccini, C. Peters, J. Roether, D. Eifler, S. Misra, E. Minay, Electrophoretic deposition of polyetheretherketone (PEEK) and PEEK/Bioglass® coatings on NiTi shape memory alloy wires, J. Mater. Sci. 41 (2006) 8152–8159. doi:10.1007/s10853-006-0556-z.

[35] F. Pishbin, A. Simchi, M.P.P. Ryan, A.R.R. Boccaccini, Electrophoretic deposition of chitosan/45S5 Bioglass® composite coatings for orthopaedic applications, Surf. Coatings Technol. 205 (2011) 5260–5268. doi:10.1016/j.surfcoat.2011.05.026.

[36] M. Cheong, I. Zhitomirsky, Electrodeposition of alginic acid and composite films, Colloids Surfaces A Physicochem. Eng. Asp. 328 (2008) 73–78. doi:10.1016/j.colsurfa.2008.06.019.

[37] L. Cordero-Arias, S. Cabanas-Polo, J. Gilabert, O.M. Goudouri, E. Sanchez, S. Virtanen, et al., Electrophoretic deposition of nanostructured TiO2 /alginate and TiO2 -bioactive glass/alginate composite coatings on stainless steel, Adv. Appl. Ceram. 113 (2014) 42–49. doi:10.1179/1743676113Y.0000000096.

[38] K.Y. Lee, D.J. Mooney, Alginate: Properties and biomedical applications, Prog. Polym. Sci. 37 (2012) 106–126. doi:http://dx.doi.org/10.1016/j.progpolymsci.2011.06.003.

[39] A. Joshi, S. Solanki, R. Chaudhari, D. Bahadur, M. Aslam, R. Srivastava, Multifunctional alginate microspheres for biosensing, drug delivery and magnetic resonance imaging, Acta Biomater. 7 (2011) 3955–3963. doi:http://dx.doi.org/10.1016/j.actbio.2011.06.053.

[40] P. Eiselt, J. Yeh, R.K. Latvala, L.D. Shea, D.J. Mooney, Porous carriers for biomedical applications based on alginate hydrogels, Biomaterials. 21 (2000) 1921–1927. doi:http://dx.doi.org/10.1016/S0142-9612(00)00033-8.

[41] I. Corni, M.P. Ryan, A.R. Boccaccini, Electrophoretic deposition: From traditional ceramics to nanotechnology, J. Eur. Ceram. Soc. 28 (2008) 1353–1367. doi:10.1016/j.jeurceramsoc.2007.12.011.

[42] K. Kanamura, J. Hamagami, Innovation of novel functional material processing technique by using electrophoretic deposition process, Solid State Ionics. 172 (2004) 303–308. doi:10.1016/j.ssi.2004.01.039.

[43] L. Besra, M. Liu, A review on fundamentals and applications of electrophoretic deposition (EPD), Prog. Mater. Sci. 52 (2007) 1–61. doi:10.1016/j.pmatsci.2006.07.001.

[44] T. Kokubo, Apatite formation on surfaces of ceramics, metals and polymers in body environment, Acta Mater. 46 (1998) 2519–2527. doi:http://dx.doi.org/10.1016/S1359-6454(98)80036-0.

[45] L. Cordero-Arias, S. Cabanas-Polo, H.X. Gao, J. Gilabert, E. Sanchez, J. a. Roether, et al., Electrophoretic deposition of nanostructured-TiO2/chitosan composite coatings on stainless steel, RSC Adv. 3 (2013) 39–41. doi:10.1039/c3ra40535d.

[46] V. Mouriño, P. Newby, A.R. Boccaccini, Preparation and Characterization of Gallium Releasing 3-D Alginate Coated 45S5 Bioglass® Based Scaffolds for Bone Tissue Engineering, Adv. Eng. Mater. 12 (2010) B283–B291. doi:10.1002/adem.200980078.

[47] R.Y.M. Huang, R. Pal, G.Y. Moon, Characteristics of sodium alginate membranes for the pervaporation dehydration of ethanol–water and isopropanol–water mixtures, J. Memb. Sci. 160 (1999) 101–113. doi:http://dx.doi.org/10.1016/S0376-7388(99)00071-X.

[48] O.P. Filho, G.P. Latorre, L.L. Hench, G.P. La Torre, L.L. Hench, Effect of crystallization on apatite-layer formation of bioactive glass 45S5, J. Biomed. Mater. Res. 30 (1996) 509–514. doi:10.1002/(SICI)1097-4636(199604)30:4<509::AID-JBM9>3.0.CO;2-T.

[49] J. Sawai, H. Igarashi, A. Hashimoto, T. Kokugan, M. Shimizu, Effect of particle size and heating temperature of ceramic powders on antibacterial activity of their slurries, J. Chem. Eng. Japan. 29 (1996) 251–256.

[50] J. Sawai, H. Igarashi, A. Hashimoto, T. Kokugan, M. Shimizu, Evaluation of growth inhibitory effect of ceramics powder slurry on bacteria by conductance method, J. Chem. Eng. Japan. 28 (1995) 288–293.

[51] J. Sawai, E. Kawada, F. Kanou, H. Igarashi, A. Hashimoto, T. Kokugan, et al., Detection of active oxygen generated from ceramic powders having antibacterial activity, J. Chem. Eng. Japan. 29 (1996) 627–633.

[52] O. Yamamoto, Influence of particle size on the antibacterial activity of zinc oxide, Int. J. Inorg. Mater. 3 (2001) 643–646. doi:10.1016/S1466-6049(01)00197-0.

[53] J. Sawai, H. Kojima, H. Igarashi, A. Hashimoto, S. Shoji, A. Takehara, et al., Escherichia coli damage by ceramic powder slurries, J. Chem. Eng. Japan. 30 (1997) 1034–1039.

[54] J. Sawai, S. Shoji, H. Igarashi, A. Hashimoto, T. Kokugan, M. Shimizu, et al., Hydrogen peroxide as an antibacterial factor in zinc oxide powder slurry, J. Ferment. Bioeng. 86 (1998) 521–522. doi:10.1016/S0922-338X(98)80165-7.

[55] P.K. Stoimenov, R.L. Klinger, G.L. Marchin, K.J. Klabunde, Metal Oxide Nanoparticles as Bactericidal Agents, Langmuir. 18 (2002) 6679–6686. doi:10.1021/la0202374.

HIGHLIGHTS

1) Organic-inorganic nanocomposite coatings fabricated by electrophoretic deposition
2) nZnO and bioactive glass containing alginate coatings exhibit antibacterial effect
3) Bioactive character and anticorrosion function of coatings demonstrated